Available online at www.sciencedirect.com
SCIENCE DIRECT®
Synthetic Metals 148 (2005) 133–139
SYNTHETIC METALS
www.elsevier.com/locate/synmet

Fluorene-based oxadiazoles: thermally stable electron-transporting materials for light-emitting devices

Fang-Iy Wu[a], Ching-Fong Shu[a,*], Chin-Hsiung Chien[b], Yu-Tai Tao[b]

[a] *Department of Applied Chemistry, National Chiao Tung University, Hsin-Chu 30035, Taiwan*
[b] *Institute of Chemistry, Academia Sinica, Taipei 11529, Taiwan*

Received 12 January 2004; received in revised form 18 August 2004; accepted 12 September 2004
Available online 11 November 2004

Abstract

We have synthesized and characterized a series of fluorene-based oxadiazole derivatives, in each of which two identical oxadiazole moieties are linked to a fluorene unit via an sp^3-hybridized carbon atom (C-9) to form a rigid, nonplanar structure. This structural feature leads to a reduction in the tendency to crystallize and an increase in the glass transition temperature. Electrochemical studies revealed that these materials undergo reversible reductions and have high electron affinities. Each fluorene-based oxadiazole exhibited reasonably good performance when it was used as the electron-transporting layer in a multi-layer organic EL device.

Keywords: Oxadiazole; Fluorene; Electron-transporting material; OLED

1. Introduction

Since the discovery of multi-layered organic light-emitting diodes (OLEDs) by Tang and Van Slyke [1] electroluminescent devices have been the subjects of intensive investigations because of their applications in full-color displays [2]. Recently, various studies have focused on improving the durability of OLEDs. A considerable amount of evidence indicates that an amorphous thin film (in OLEDs) having a high glass transition temperature (T_g) is less vulnerable to heat-induced morphological change and, hence, the device's performance becomes more stable [3]. Thus, high-T_g materials are always desirable for applications in OLEDs. Several distinct classes of glass-forming small molecules that have elevated values of T_g have been synthesized, including spiro-shaped, "star-burst", dendritic, tetrahedral, and cardo molecules [4–8].

It has been demonstrated that incorporating a cyclic cardo side group, such as fluorene unit, into a polymer affords amorphous, aromatic polyimides and polyamides with high values of T_g [9]. Recently, one of us reported a fluorene-containing triarylamine derivative as an amorphous, hole-transporting material with a high value of T_g that exhibited superior performance when incorporated in electroluminescent devices [8b]. Owing to their electron-deficient nature, molecular and polymeric derivatives of oxadiazole have been explored in this context as electron-transporting materials [6a,b,10,11]. Herein, we report the synthesis and characterization of high-T_g and efficient electron-transporting materials, in each of which two identical oxadiazole moieties – the electron-transporting functionalities – are connected to a fluorene unit via an sp^3-hybridized carbon atom (C-9) to form a rigid 3D structure. We report also the fabrication and performance of blue-emitting OLEDs using these oxadiazole-based substances as the electron-transporting materials. Because of the sterically demanding nature of the sp^3-hybridized carbon atom, the presence of the fluorene unit not only hinders intermolecular close packing but it also increases the molecule's rigidity, which results in amorphous glassy materials that have improved thermal stabilities. In addition, the tetrahedral nature of the C-9 carbon

* Corresponding author. Tel.: +886 35 712121; fax: +886 35 723764.
E-mail address: shu@cc.nctu.edu.tw (C.-F. Shu).

0379-6779/$ – see front matter © 2004 Elsevier B.V. All rights reserved.
doi:10.1016/j.synthmet.2004.09.029

atom connects the conjugated oxadiazole moieties through a σ-bonded network, which in turn can serve as a conjugation interrupt, and, thus, most of the desired electronic and optical properties of the corresponding oxadiazole are preserved.

2. Experimental section

2.1. General directions

9,9-Bis(4-cyanophenyl)fluorene (**1**) and 9,9-bis(4-tetraazolylphenyl)fluorene (**2**) were synthesized according to literature procedures [11f]. The solvents were dried using standard procedures. All other reagents were used as received from commercial sources, unless otherwise stated. ^{1}H and ^{13}C NMR spectra were recorded on a Varian Unity 300 MHz and a Bruker-DRX 300 MHz spectrometer. Mass spectra were obtained on a JEOL JMS-SX 102A mass spectrometer. Differential scanning calorimetry (DSC) was performed on a SEIKO EXSTAR 6000DSC unit using a heating rate of 20 °C min^{-1} and a cooling rate of 40 °C min^{-1}. Samples were scanned from 30 to 370 °C, cooled to 10 °C, and then scanned again from 30 to 370 °C. The glass transition temperatures (T_g) were determined from the second heating scan. Thermogravimetric analysis (TGA) was undertaken on a DuPont TGA 2950 instrument. The thermal stability of the samples was determined under a nitrogen atmosphere, by measuring the weight loss while heating at a rate of 20 °C min^{-1}. UV–visible spectra were measured with an HP 8453 diode-array spectrophotometer. Photoluminescence (PL) spectra were obtained on a Hitachi F-4500 luminescence spectrometer. The PL quantum yields (Φ_f) of oxadiazole derivatives were determined relative to that of 2-phenyl-5-(4-biphenyl)-1,3,4-oxadiazole in benzene ($\Phi_f = 0.8$) [12]. Cyclic voltammetry (CV) and differential pulse voltammetry (DPV) measurements were performed on a BAS 100 B/W electrochemical analyzer. The oxidation and reduction measurements were carried out, respectively, in anhydrous CH_2Cl_2 and anhydrous THF containing 0.1 M tetrabutylammonium hexafluorophosphate ($TBAPF_6$) as the supporting electrolyte at a scan rate of 50 mV s^{-1}. The potentials were measured against an Ag/Ag^+ (0.01 M $AgNO_3$) reference electrode using ferrocene as the internal standard. The onset potentials were determined from the intersection of two tangents drawn at the rising current and background current of the cyclic voltammogram.

2.2. 9,9-Bis(4-(5-(4-tert-butylphenyl)-2-oxadiazolyl)phenyl)fluorene (*3a*)

4-*tert*-Butylbenzoyl chloride (1.9 mL, 9.9 mmol) was added dropwise to a solution of compound **2** (1.50 g, 3.3 mmol) in pyridine (8.0 mL) at 25 °C. The reaction mixture was heated at 125 °C for 3 h. After cooling, the solution was poured into a mixture of water and MeOH (1:3, 150 mL). The resulting precipitate was collected by filtration, washed with water, and dried. The product was purified by column chromatography using $CHCl_3$ as the eluent followed by recrystallization from toluene/$CHCl_3$ (5:1) to yield **3a** (2.12 g, 89.3%). ^{1}H NMR (300 MHz, $CDCl_3$): δ 1.34 (s, 18H), 7.31 (ddd, J = 7.3, 7.3, 1.2 Hz, 2H), 7.36 (d, J = 8.6 Hz, 4H), 7.37–7.45 (m, 4H), 7.52 (d, J = 8.6 Hz, 4H), 7.81 (d, J = 7.4 Hz, 2H), 8.00 (d, J = 8.6 Hz, 4H), 8.01 (d, J = 8.6 Hz, 4H). ^{13}C NMR (75 MHz, $CDCl_3$): δ 31.0, 35.0, 65.5, 120.5, 121.0, 122.7, 125.9, 126.0, 126.7, 127.0, 128.1, 128.2, 128.7, 140.2, 149.2, 149.7, 155.3, 164.0, 164.6. HRMS $[M+H]^+$: calcd. for $C_{49}H_{43}N_4O_2$: 719.3386, found 719.3392. Anal. Calcd. for $C_{49}H_{42}N_4O_2$: C, 81.86; H, 5.89; N, 7.80. Found: C, 81.87; H, 6.09; N, 7.94.

2.3. 9,9-Bis(4-(5-(1-naphthyl)-2-oxadiazolyl)phenyl) fluorene (*3b*)

Compound **3b** was prepared (88.7%) from compound **2** and 1-naphthoyl chloride following the procedure described for the preparation of **3a**. ^{1}H NMR (300 MHz, $CDCl_3$): δ 7.33 (ddd, J = 7.5, 7.5, 1.3 Hz, 2H), 7.39–7.48 (m, 4H), 7.41 (d, J = 8.6 Hz, 4H), 7.51–7.60 (m, 4H), 7.66 (ddd, J = 7.7, 7.7, 1.5 Hz, 2H), 7.83 (d, J = 7.6 Hz, 2H), 7.90 (d, J = 7.8 Hz, 2H), 8.00 (d, J = 8.2 Hz, 2H), 8.07 (d, J = 8.6 Hz, 4H), 8.21 (dd, J = 7.3, 1.1 Hz, 2H), 9.25 (d, J = 8.2 Hz, 2H). ^{13}C NMR (75 MHz, $CDCl_3$): δ 65.5, 120.4, 120.6, 122.5, 124.8, 126.0, 126.1, 126.7, 127.2, 128.1, 128.2, 128.3, 128.6, 128.8, 130.0, 132.6, 133.8, 140.2, 149.4, 149.6, 163.8, 164.5. HRMS $[M+H]^+$: calcd. for $C_{49}H_{31}N_4O_2$ 707.2447, found 707.2454. Anal. Calcd. for $C_{49}H_{30}N_4O_2$: C, 83.26; H, 4.28; N, 7.93. Found: C, 83.14; H, 4.49; N, 7.68.

2.4. 9,9-Bis(4-(5-(2-naphthyl)-2-oxadiazolyl)phenyl) fluorene (*3c*)

Compound **3c** was prepared (66.3%) from compound **2** and 2-naphthoyl chloride following the procedure described for the preparation of **3a**. ^{1}H NMR (300 MHz, $CDCl_3$): δ 7.33 (ddd, J = 7.4, 7.4, 1.2 Hz, 2H), 7.39–7.46 (m, 4H), 7.40 (d, J = 8.6 Hz, 4H), 7.52–7.61 (m, 4H), 7.83 (d, J = 7.6 Hz, 2H), 7.86–7.91 (m, 2H), 7.93–7.97 (m, 2H), 7.96 (d, J = 8.6 Hz, 2H), 8.07 (d, J = 8.6 Hz, 4H), 8.17 (dd, J = 8.6, 1.4 Hz, 2H), 8.58 (d, J = 1.4 Hz, 2H). ^{13}C NMR (75 MHz, $CDCl_3$): δ 65.7, 120.7, 121.1, 122.7, 123.2, 126.1, 127.2, 127.3, 127.4, 128.1, 128.3, 128.4, 128.9, 129.1, 132.9, 134.8, 140.4, 149.5, 149.8, 164.4, 164.8. HRMS $[M+H]^+$: calcd. for $C_{49}H_{31}N_4O_2$ 707.2447, found 707.2451. Anal. Calcd. for $C_{49}H_{30}N_4O_2$: C, 83.26; H, 4.28; N, 7.93. Found: C, 82.94; H, 4.55; N, 7.87.

2.5. Fabrication of light-emitting devices

The hole-transport materials 4,4′-bis[*N*-(1-naphthyl)-*N*-phenylamino]biphenyl (NPB), 4,4′-dicarbazolyl-1,1′-

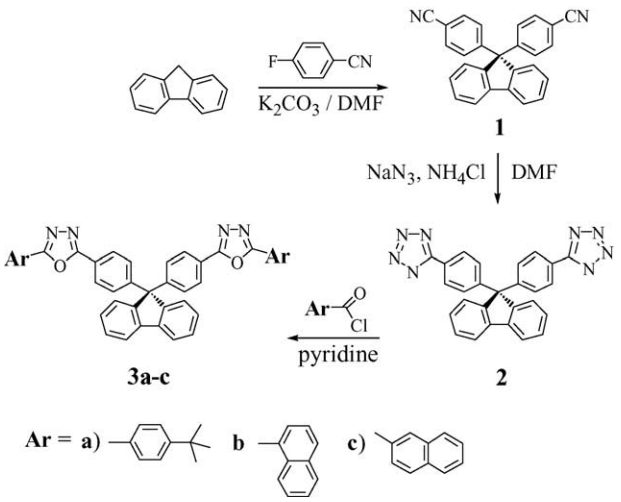

Scheme 1.

biphenyl (CBP) and electron-transport material 1,3,5-tris(*N*-phenylbenzimidazol-2-yl)benzene (TPBI) were sublimed through a temperature-gradient sublimation system. Pre-patterned ITO glasses with active device areas of 3.14 mm^2 were thoroughly cleaned by sonication in detergent, ethanol, and DI water, respectively, for 5 min. After blowing dry with a stream of nitrogen, the glasses were than treated with oxygen plasma for 3 min. The glasses were then loaded into an Ulvac Cryogenic deposition system, which was then evacuated to a pressure below $\sim 2 \times 10^{-5}$ Torr. All of the organic layers were deposited at a rate of 1.5–2.5 Å/s. An alloy of magnesium and silver (ca. 10:1, 50 nm) was deposited as the cathode, followed by a silver cap (1000 Å). The current–voltage luminance of each device was measured with a Keithley 2400 Source meter and a Newport 1835C optical meter equipped with an 818ST silicon photodiode.

3. Results and discussion

3.1. Synthesis

Scheme 1 illustrates the synthetic route followed for the preparation of the fluorene-based 1,3,4-oxadiazole compounds **3a**–**c**. There are two general approaches for the synthesis of oxadiazole derivatives: cyclocondensation of acyl hydrazides and ring transformation of acylated tetrazoles [13,14]. The relatively high yields and facile workup procedures render the tetrazole route more attractive for the preparation of pure oxadiazole derivatives [15]. Starting from fluorene, which contains an activated methylene group at the C-9 position, 9,9-bis(4-cyanophenyl)fluorene (**1**) [11f] was prepared by nucleophilic aromatic substitution of 4-fluorobenzonitrile with the fluorenyl anion generated by reaction with K_2CO_3 in DMF. By reacting with sodium azide, compound **1** was converted to the tetrazole derivative **2** [11f], which was subsequently transformed into the desired oxadiazole derivatives **3a**–**c** by reacting with aroyl chlorides in pyridine under reflux. The chemical structures of the obtained oxadiazoles **3a**–**c** were confirmed by ^1H and ^{13}C NMR spectroscopy. Data from high-resolution mass spectrometry and elemental analyses also verified their structures.

Table 1
Thermal properties of the fluorene-based oxadiazole derivatives

Compound	DSC (°C)[a]			TGA (°C)[b]	
	T_g[c]	T_c	T_m	5 wt.% loss	10 wt.% loss
3a	162	239	307	454	468
3b	138	n.a.	n.a.	440	454
3c	156	220	315	447	466
PBD	n.a.	64	142		

[a] Measured at a heating rate of 20 °C min^{-1} and a cooling rate of 40 °C min^{-1}; n.a.: not available.
[b] Measured at a heating rate of 20 °C min^{-1} under a nitrogen atmosphere.
[c] Determined during the second heating.

3.2. Thermal properties

The thermal properties of oxadiazoles **3a**–**c** were investigated by differential scanning calorimetry (DSC) and thermogravimetric analysis (TGA); the results are presented in Table 1. Fig. 1 displays the DSC curves of **3a**–**c**. In the first heating cycle, endothermic peaks are observed at 307 and 315 °C; these peaks are due to the melting of **3a** and **3c**, respectively. No melting point was detected for **3b**. In subsequent heating cycles, each oxadiazole exhibits a distinct glass transition temperature (T_g) in the range 138–162 °C, but does not undergo recrystallization or melting. In contrast, a related analogue, 2-(4-biphenyl)-5-(4-*tert*-butylphenyl)-1,3,4-oxadiazole (**PBD**), melts already at 142 °C. We attribute the pronounced morphological stability in oxadiazoles **3a**–**c** to the nonplanar, 3D cardo-structure that arises from the incorporation of the fluorene moiety [8,16]. In addition, the higher molecular weights of oxadiaxoles **3a**–**c**, relative to **PBD**, may also account for their higher melting points. It has been shown that morphological changes that result from the thermal instability of amorphous organic layers lead to the degradation of EL devices [4]. Devices having a long lifetime require the

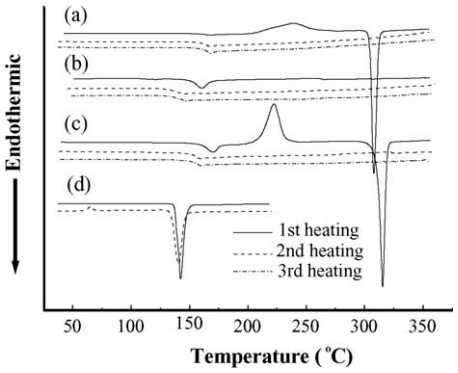

Fig. 1. DSC thermograms, with sequential heating and cooling cycles of: (a) **3a**, (b) **3b**, (c) **3c**, and (d) **PBD**.

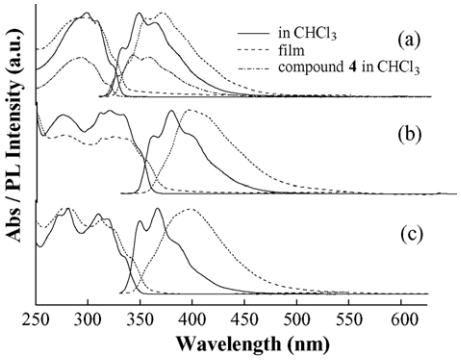

Fig. 2. UV–vis absorption and PL spectra, in chloroform solutions and as thin films of: (a) **3a**, (b) **3b**, and (c) **3c**; also depicted in (a) are the UV–vis absorption and PL spectra of model compound **4** in a chloroform solution.

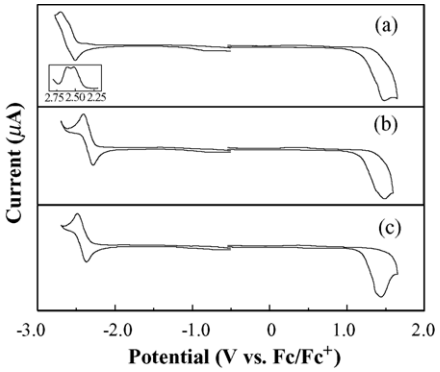

Fig. 3. Cyclic voltammograms of: (a) **3a**, (b) **3b**, and (c) **3c**; inset (a): differential pulse voltammetry of **3a** in the reduction region.

molecules used in the OLED to have a relatively high values of T_g (T_m). In addition to their high glass transition temperatures, compounds **3a–c** exhibit good film-forming properties and high thermal stabilities. As revealed by TGA, their 5 wt.% loss temperatures under a nitrogen atmosphere are up to 440 °C.

3.3. Photophysical properties

Fig. 2 displays the solution and thin film absorption and photoluminescence (PL) spectra of oxadiazoles **3a–c**; their spectral properties are summarized in Table 2. In chloroform solution, **3a** exhibits an absorption in the range 299–324 nm that results from a π–π^* transition, while the emission spectrum displays a vibronic fine structure with three bands at 333, 348, and 364 nm. Compared with **3a**, the absorption (emission) spectra of **3b** and **3c** are red-shifted by 24 (30) and 11 (19) nm, respectively, as a result of the increase in conjugation length. As illustrated in Fig. 2a, the solution UV–vis absorption and PL spectra of a model compound, 2,5-di[4-(*tert*-butyl)phenyl]-1,3,4-oxadiazole (**4**), which is a monomeric oxadiazole, are almost superimposable with those of **3a**. This observation indicates that the tetrahedrally bonded carbon atom (C-9) of the fluorene unit serves as a conjugation interrupt and that the π systems of the two connected oxadiazole moieties have little or no interaction with one another. The solution fluorescence quantum yields (Φ_f) of **3a–c** and **4**, all of which fall in the range Φ_f = 0.60–0.74, were determined relative to that of 2-phenyl-5-(4-biphenyl)-1,3,4-oxadiazole in benzene (Φ_f = 0.80) [12]. By comparison with their corresponding spectra in dilute solutions, the emission spectra of films of **3a–c** are relatively structureless and are red-shifted by 22–30 nm.

3.4. Electrochemistry

The electrochemical behavior of oxadiazoles **3a–c** was investigated by cyclic voltammetry using ferrocene as the internal standard. Fig. 3 displays the cyclic voltammograms of **3a–c** and the data are tabulated in Table 3. During the cathodic scan, **3a** exhibits two poorly resolved, reversible reductions with the onset potential at −2.48 V. Differential pulse voltammetry (DPV) clearly shows the appearance of two distinguishable reductions at −2.51 and −2.61 V ($E^{\circ\prime}$). The relatively small potential difference in the reduction indicates that the mono-anionic species generated during the first reduction may not delocalize the charge efficiently over the two oxadiazole moieties, which are connected through an sp^3-hybridized carbon atom. With **3b** and **3c**, only one reversible reduction is observed in each case, with formal reduction potentials ($E^{\circ\prime}$) at −2.34 and −2.42 V, respectively, and onset potentials at −2.25 and −2.31 V, respectively. Upon the anodic sweep, **3a–c** show irreversible oxidation processes with onset potentials at 1.18, 1.17, and 1.19 V, respectively. Based on the onset potentials for the oxidation and reduction, the HOMO and LUMO energy levels of oxadiazoles **3a–c** were estimated with regard to the energy level of the

Table 2
Optical properties of the fluorene-based oxadiazole derivatives

Compound	Absorption (nm)		Emission (nm)		Φ_f (%)[a]
	Solution[b]	Film[c]	Solution[b]	Film[c]	
3a	299, 308, 324	298, 309, 325	333, 348, 364	355, 370, 392	74
3b	320, 332, 346	324, 337, 354	361, 378, 396	403	65
3c	310, 319, 334	312, 322, 340	349, 367, 384	397	60
4	294, 304, 318		329, 343, 357		73

[a] Φ_f: fluorescence quantum efficiency, relative to 2-phenyl-5-(4-biphenyl)-1,3,4-oxadiazole in benzene (Φ_f = 0.8).
[b] Evaluated in a chloroform solution.
[c] Measured in the solid state on a quartz plate.

Table 3
Electrochemical properties of the fluorene-based oxadiazole derivatives

Compound	E_{onset}[a] (V)		Energy levels (eV)		Bandgap energy (eV)	
	n-Doping	*p*-Doping	LUMO[b]	HOMO[c]	E_{ele}[d]	E_{opt}[e]
3a	−2.48	1.18	2.32	5.98	3.66	3.73
3b	−2.25	1.17	2.55	5.97	3.42	3.44
3c	−2.31	1.19	2.49	5.99	3.50	3.55

[a] Measured vs. ferrocene/ferrocenium.
[b] LUMO = 4.8 + E_{onset}(*n*-doping).
[c] HOMO = 4.8 + E_{onset}(*p*-doping).
[d] E_{ele} = HOMO − LUMO.
[e] E_{opt}: the bandgap energy estimated from the onset wavelength of the optical absorption.

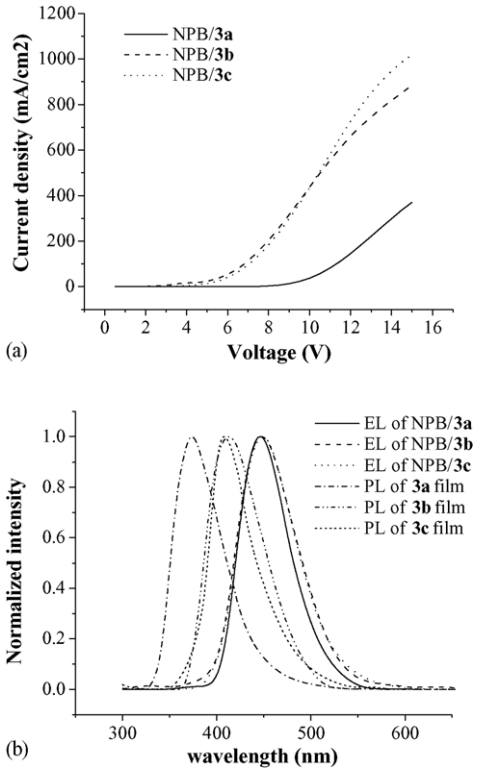

Fig. 4. (a) Plot of current density vs. voltage and (b) EL spectra of the devices ITO/NPB/**3a**–**c**/Mg:Ag, and solid PL spectra of films of **3a**–**c**.

FOC reference (4.8 eV below the vacuum level) [17]; the values are summarized in Table 3. The band gaps of oxadiazoles **3a**–**c** estimated from these electrochemical measurements are in agreement with the results determined from the optical absorption threshold. From their reversible reductions and high electron affinities, it would appear that oxadiazoles **3a**–**c** have the potential for use as electron-transporting materials in organic LEDs.

3.5. Electroluminescent devices

Two types of EL devices, in which compounds **3a**–**c** served as electron-transport materials, were fabricated to assess their transporting properties. Firstly, we prepared standard two-layer devices with the configuration ITO/NPB (40 nm)/**3a**–**c** (40 nm)/Mg:Ag (Table 4). Fig. 4 displays the *I*–*V* characteristics for the devices made from the three derivatives. We see that **3b** and **3c** both gave higher current densities than did **3a**. At a driving voltage of 10 V, a current density of 500 mA/cm^2 was reached. This value is comparable to that obtained when using another typical electron-transporting material, TPBI [18], but it is smaller than that obtained from an Alq-based device. The EL spectra of the two-layer devices differ from their respective PL spectra in that they all have λ_{max} located at ca. 448 nm, the same value as that observed in the PL spectrum of NPB. This result indicates that, in a manner similar to that of TPBI, **3a**–**c** serve as hole blockers in the current device structures because of the large energy barrier between the HOMO of NPB and those of **3a**–**c**, which prevents the holes from injecting into the **3a**–**c** layer (Fig. 5). Instead, the smaller barrier between the LUMOs of these materials and that of NPB results in a recombination zone located mainly within the NPB layer. The blue devices, while unoptimized, exhibited maximum brightnesses between 450 and 1600 cd/m^2 and external quantum efficiencies between 0.2 and 0.3% (Table 4).

Secondly, we prepared three three-layer devices, each of which incorporated a compound **3a**–**c** as the electron-transporting layer and a blue dye PAP-NPA [19] inserted between the NPB and **3** layers. Previously, the PAP-NPA

Table 4
Performance of the ITO/NPB (40 nm)/**3a**–**c** (40 nm)/Mg:Ag devices

Device structure	λ_{max} (nm)	Maximum luminescence (cd/m^2)	QE (%)[a]	Luminescent efficiency (cd/A)[a]	Power efficiency (lm/W)[a]	CIE (*x*, *y*)
NPB/**3a**	448	448	0.33	0.19	0.054	0.14, 0.06
NPB/**3b**	448	867	0.20	0.17	0.078	0.15, 0.10
NPB/**3c**	448	1600	0.25	0.22	0.098	0.15, 0.10

[a] At current density = 100 mA/cm^2.

Table 5
Performance of the ITO/NPB/PAP-NPA/**3a–c**/Mg:Ag devices

Layer structure[a]	λ_{max} (nm)	Maximum luminescence (cd/m^2)	QE (%)[b]	Luminescent efficiency (cd/A)[b]	Power efficiency (lm/W)[b]	CIE (x, y)
NPB/PAP-NPA/**3a**	454	5399	1.47	1.29	0.49	0.14, 0.10
NPB/PAP-NPA/**3b**	454	6076	1.54	1.39	0.62	0.15, 0.10
NPB/PAP-NPA/**3c**	454	7173	1.75	1.57	0.68	0.14, 0.10
NPB/PAP-NPA/TPBI	452	16760	2.36	2.06	1.07	0.15, 0.10

[a] At current density = 100 mA/cm^2.
[b] Device configuration is NPB (40 nm)/PAP-NPA (10 nm)/**3a–c** or TPBI (30 nm).

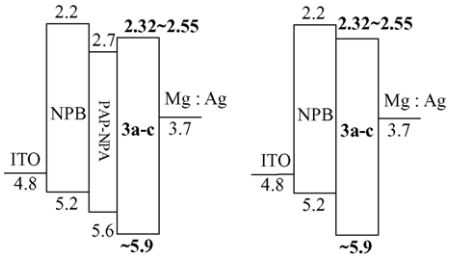

Fig. 5. Energy alignment of the various layers in the devices ITO/NPB/**3a–c** and ITO/NPB/PAP-NPA/**3a–c**.

dye was found to give a strong blue emission from a device having the structure ITO/NPB (40 nm)/PAP-NPA (10 nm)/TPBI (30 nm)/Mg:Ag [19]. Here, with similar device configurations of ITO/NPB (40 nm)/PAP-NPA (10 nm)/**3a–c** (30 nm), all three devices displayed the same EL spectra, with λ_{max} = 454 nm resulting from PAP-NPA, with CIE coordinates around (0.15, 0.10) (Fig. 6). Thus **3a–c** successfully transported electrons from the cathode into the PAP-NPA layer, where they were recombined with the holes. This situation is reasonable in view of the alignments of the energy levels of the various layers (Fig. 5). Fig. 7 shows the *I–V* characteristics for these devices together with a reference device that used TPBI as the electron-transporting material. The current densities for the **3**-based devices were lower than that for the TPBI-based one. This observation may be a result of lower electron mobility in **3a–c** relative to TPBI. Table 5 presents the performance characteristics for the **3**-based devices. The external quantum efficiencies ranged between 1.4 and 1.7% and the maximum brightness reached ca. 5400–7000 cd/m^2.

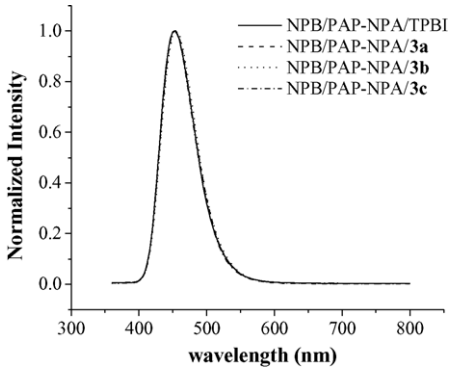

Fig. 6. EL spectra of the devices NPB/PAP-NPA/TPBI and NPB/PAP-NPA/**3a–c**.

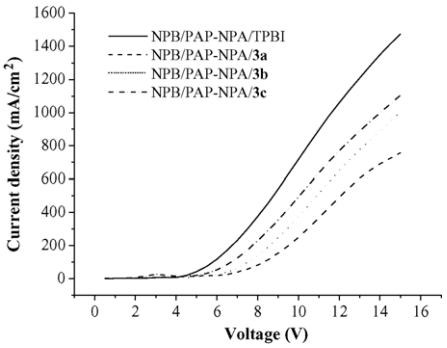

Fig. 7. Plot of current density vs. voltage for the devices ITO/NPB/PAP-NPA/**3a–c**/Mg:Ag and ITO/NPB/PAP-NPA/TPBI/Mg:Ag.

In summary, we have synthesized and characterized a series of fluorene-based oxadiazole derivatives. These compounds exhibited high values of T_g and thermal stability, presumably because of the incorporation of the fluorene units as linkers between the two oxadiazole fragments. Nevertheless, these derivatives preserve the optical and electrochemical characteristics of their pristine oxadiazole units. Reasonably good EL performances were obtained when these materials were used as the electron-transporting layer in both two- and three-layer device configurations. Further modification and optimization of the structures and devices currently are in progress.

Acknowledgment

We thank the National Science Council of the Republic of China for financial support.

References

[1] C.W. Tang, S.A. Van Slyke, Appl. Phys. Lett. 51 (1987) 913.
[2] (a) S. Miyata, H.S. Nalwa (Eds.), Organic Electroluminescent Materials and Devices, Gordon and Breach Publishers, New York, 1997;
(b) C.H. Chen, J. Shi, C.W. Tang, Macromol. Symp. 125 (1997) 1;
(c) C.H. Chen, J. Shi, C.W. Tang, Coord. Chem. Rev. 171 (1998) 161;
(d) U. Mitschke, P. Bauerle, J. Mater. Chem. 10 (2000) 1471;
(e) L.S. Hung, C.H. Chen, Mater. Sci. Eng. R 39 (2002) 143.
[3] (a) S. Tokito, H. Tanaka, K. Noda, A. Okada, Y. Taga, Appl. Phys. Lett. 70 (1997) 1929;
(b) J. Salbeck, N. Yu, J. Bauer, F. Weissörtel, H. Bestgen, Synth. Met. 91 (1997) 209;

(c) B.E. Konne, D.E. Loy, M.E. Thompson, Chem. Mater. 10 (1998) 2235;
(d) D.F. O'Brien, P.E. Burrows, S.R. Forrest, B.E. Konne, D.E. Loy, M.E. Thompson, Adv. Mater. 10 (1998) 1108;
(e) F. Steuber, J. Staudigel, M. Stössel, J. Simmerer, A. Winnacker, H. Spreitzer, F. Weissörtel, J. Salbeck, Adv. Mater. 12 (2000) 130;
(f) Y. Shirota, J. Mater. Chem. 10 (2000) 1;
(g) P. Strohriegl, J.V. Grazulevicius, Adv. Mater. 14 (2002) 1439.

[4] (a) J. Salbeck, J. Bauer, F. Weissörtel, Macromol. Symp. 125 (1997) 121;
(b) N. Johansson, D.A. dos Santos, S. Guo, J. Cornil, M. Fahlman, J. Salbeck, H. Schenk, H. Arwin, J.L. Brédas, W.R. Salenek, J. Chem. Phys. 107 (1997) 2542;
(c) N. Johansson, J. Salbeck, J. Bauer, F. Weissörtel, P. Bröms, A. Andersson, W.R. Salaneck, Adv. Mater. 10 (1998) 1136;
(d) Y.H. Kim, D.C. Shin, S.H. Kim, C.H. Ko, H.S. Yu, Y.S. Chae, S.K. Kwon, Adv. Mater. 13 (2001) 1690;
(e) C.C. Wu, Y.T. Lin, H.H. Chiang, T.Y. Cho, C.W. Chen, K.T. Wong, Y.L. Liao, G.H. Lee, S.M. Peng, Appl. Phys. Lett. 81 (2002) 577.

[5] (a) H. Inada, Y.J. Shirota, Mater. Chem. 3 (1993) 319;
(b) E. Ueta, H. Nakano, Y. Shirota, Chem. Lett. (1994) 2397;
(c) H. Kageyama, K. Itano, W. Ishikawa, Y. Shirota, J. Mater. Chem. 6 (1996) 675;
(d) M. Thelakkat, H. Schmidt, Adv. Mater. 10 (1998) 219;
(e) I.Y. Wu, J.T. Lin, Y.T. Tao, E. Balasubramaniam, Y.Z. Su, C.W. Ko, Chem. Mater. 13 (2001) 2626.

[6] (a) J. Bettenhausen, P. Strohriegl, Adv. Mater. 8 (1996) 507;
(b) J. Bettenhausen, M. Greczmiel, M. Jandke, P. Strohriegl, Synth. Met. 91 (1997) 223;
(c) S. Tanaka, T. Iso, Y. Doke, Chem. Commun. (1997) 2063;
(d) H. Meier, M. Lehmann, Angew. Chem., Int. Ed. Engl. 37 (1998) 643;
(e) Y. Sakamoto, T. Suzuki, A. Miura, H. Fujikawa, S. Tokito, Y. Taga, J. Am. Chem. Soc. 122 (2000) 1832.

[7] (a) M.R. Robinson, S. Wang, G.C. Bazan, Y. Cao, Adv. Mater. 12 (2000) 1701;
(b) S. Wang, W.J. Oldham Jr., R.A. Hudack Jr., G.C. Bazan, J. Am. Chem. Soc. 122 (2000) 5695;
(c) L.H. Chan, H.C. Yeh, C.T. Chen, Adv. Mater. 13 (2001) 1637;
(d) H.C. Yeh, R.H. Lee, L.H. Chan, T.Y.J. Lin, C.T. Chen, E. Balasubramaniam, Y.T. Tao, Chem. Mater. 13 (2001) 2788.

[8] (a) K.T. Wong, Z.J. Wang, Y.Y. Chien, C.L. Wang, Org. Lett. 3 (2001) 2285;
(b) C.W. Ko, Y.T. Tao, Synth. Met. 126 (2002) 37.

[9] (a) C.P. Yang, J.H. Lin, Polym. Sci., Part A: Polym. Chem. 31 (1993) 2153;
(b) S.H. Hsiao, C.T. Li, J. Polym. Sci., Part A: Polym. Chem. 37 (1999) 1403;
(c) S.H. Hsiao, C.P. Yang, W.L. Lin, Macromol. Chem. Phys. 200 (1999) 1428.

[10] (a) J. Kido, H. Shionoya, K. Nagai, Appl. Phys. Lett. 67 (1995) 2281;
(b) S. Janietz, A. Wedel, Adv. Mater. 9 (1997) 403;
(c) N. Tamoto, C. Adachi, K. Nagai, Chem. Mater. 9 (1997) 1077.

[11] (a) M. Greczmiel, P. Strohriegl, M. Meier, W. Brütting, Macromolecules 30 (1997) 6042;
(b) Z. Peng, J. Zhang, Chem. Mater. 11 (1999) 1138;
(c) X. Jiang, R.A. Register, K.A. Killeen, M.E. Thompson, F. Pschitzka, J.C. Sturm, Chem. Mater. 12 (2000) 2542;
(d) M. Zheng, L. Ding, E.E. Gürel, P.M. Lahti, F.E. Karasz, Macromolecules 34 (2001) 4124;
(e) J. Ding, M. Day, G. Robertson, J. Roovers, Macromolecules 35 (2002) 3474;
(f) F.-I. Wu, D.S. Reddy, C.-F. Shu, M.S. Liu, A.K.-Y. Jen, Chem. Mater. 15 (2003) 269.

[12] J.N. Demas, G.A. Crosby, J. Phys. Chem. 75 (1971) 991.

[13] E. Klingsberg, J. Am. Chem. Soc. 80 (1958) 5786.

[14] R. Huisgen, J. Sauer, J.H. Sturm, J.H. Markgraf, Chem. Ber. 93 (1960) 2106.

[15] H. Detert, D. Schollmeier, Synthesis (1999) 999.

[16] S. Okutsu, T. Onikubo, M. Tamano, T. Enokida, IEEE Trans. Electron Dev. 44 (1997) 1302.

[17] J. Pommerehne, H. Vestweber, W. Guss, R.F. Mahrt, H. Bässler, M. Porsch, J. Daub, Adv. Mater. 7 (1995) 551.

[18] Y.T. Tao, E. Balasubramanian, A.B. Danel, B. Jarose, P. Tomasik, Appl. Phys. Lett. 77 (2002) 1575.

[19] Y.T. Tao, C.H. Chuen, C.W. Ko, J.W. Peng, Chem. Mater. 14 (2002) 4256.